Bifurcation of standing waves into a pair of oppositely traveling waves with oscillating amplitudes caused by a three-mode interaction

A. Pinter,* M. Lücke, and Ch. Hoffmann

Institut für Theoretische Physik, Universität des Saarlandes, Postfach 151150, D-66041 Saarbrücken, Germany

A flow state consisting of two oppositely traveling waves (TWs) with oscillating amplitudes has been found in the counter-rotating Taylor-Couette system by full numerical simulations. This structure bifurcates out of axially standing waves that are nonlinear superpositions of left- and right-handed spiral vortex waves with equal time-independent amplitudes. Beyond a critical driving, the two spiral TW modes start to oscillate in counterphase due to a Hopf bifurcation. The trigger for this bifurcation is provided by a nonlinearly excited mode of different symmetry than the spiral TWs. A three-mode coupled amplitude equation model is presented that captures this bifurcation scenario. The mode-coupling between two symmetry degenerate critical modes and a nonlinearly excited one that is contained in the model can be expected to occur in other structure-forming systems as well.

PACS number(s): 47.20.Ky, 47.20.Lz, 47.32.−y, 47.54.−r

Many nonlinear structure-forming systems that are driven out of equilibrium show a transition to traveling waves (TWs) as a result of an oscillatory instability [1]. In the presence of spatial inversion symmetry in one or more directions also a standing wave (SW) solution bifurcates which is a nonlinear superposition of the two symmetry degenerated, oppositely propagating TWs with equal amplitudes.

SWs and TWs have a common onset as a result of a primary Hopf bifurcation. But at onset only one of them is stable [2,3]. Furthermore, there are mixed patterns with nonequal amplitude combinations of the degenerated TWs that arise, e.g., via secondary bifurcations at larger driving. The variety with temporally constant, nonequal TW amplitudes can provide a stability transferring connection between TWs that, e.g., are stable at onset and SWs that become stable later on [4].

The variety in which the TW amplitudes oscillate in time is the subject of this paper. This solution bifurcates out of the SW via a Hopf bifurcation. To be concrete we investigate wave structures consisting of spiral vortices in the annular gap between counter-rotating concentric cylinders of the Taylor-Couette system [5,6]. To that end we have performed numerical simulations of the Navier-Stokes equations (NSE) to reveal the bifurcation properties as well as the spatiotemporal structure of the oscillating mixed wave states. In addition, we provide coupled three-mode amplitude equations that capture this bifurcation to explain the underlying mode-coupling mechanism. We are not aware that these states have been reported so far in the Taylor-Couette literature. Furthermore, one can expect that the mode-coupling mechanism between two symmetry degenerate critical modes and the nonlinearly excited one that is described by our coupled amplitude equations and that drives the oscillatory instability is operating in other pattern-forming systems as well.

The waves are realized by left-handed spiral vortex (L-SPI) and right-handed spiral vortex (R-SPI) structures that are mirror images of each other. The azimuthal advection by the basic circular Couette flow (CCF) rotates both like rigid

objects into the same direction as the inner cylinder [7]. As a result of the enforced rotation the phases of L-SPI and R-SPI travel axially into opposite directions. This system offers an easy experimental and numerical access to forward bifurcating TWs and SWs that are called ribbons (RIBs) [8–11] in the Taylor-Couette literature. Being a nonlinear superposition of L-SPI and R-SPI the RIB structure also rotates azimuthally, however, such that its oscillations in axial direction form a SW.

Here we elucidate how such stable SWs lose stability to an oscillating state via a Hopf bifurcation. Therein, the interaction with another nonlinearly excited, nontraveling mode induces the TW constituents of the SW, i.e., the L-SPI and the R-SPI to oscillate in counterphase around a common mean. These oscillating mixed wave states that we call oscillating cross spirals (O-CR-SPI) are quite robust. Thus, they should easily be observable in experiments.

All these spiral structures are axially and azimuthally periodic. We have focused our simulations on patterns with axial wavelength $\lambda = 1.3$ measured in units of the gap width and azimuthal wave number $M = 2$. The numerical solutions of the NSE were obtained for a system with radius ratio $\eta = 1/2$ by methods described in [7].

Control- and order parameters. The rotational velocities of the inner and outer cylinders are measured by the respective Reynolds numbers R_1 and R_2. We fix $R_1 = 240$ [12,13] and we introduce the reduced distance $\mu = (R_2 - R_2^0)/|R_2^0|$ from the common onset of SPI and RIB flow at $R_2^0 = -605.5$ as control parameter. We characterize the spatiotemporal properties of the vortex waves using the Fourier decomposition

$$f(r,\varphi,z,t) = \sum_{m,n} f_{m,n}(r,t)e^{i(m\varphi+nkz)} \tag{1}$$

in azimuthal and axial direction. Here one has $f_{-m,-n} = \overline{f_{m,n}}$ with the overbar denoting complex conjugation. Order parameters are the moduli $|A|$, $|B|$, $|C|$ and the time derivatives $\dot{\theta}_A$, $\dot{\theta}_B$, $\dot{\theta}_C$ of the phases of the dominant modes in the decomposition (1) of, say, the radial velocity u at midgap $u_{2,1} = A = |A|e^{-i\theta_A}$, $u_{2,-1} = B = |B|e^{-i\theta_B}$, and $u_{0,2} = C = |C|e^{-i\theta_C}$. Here,

---
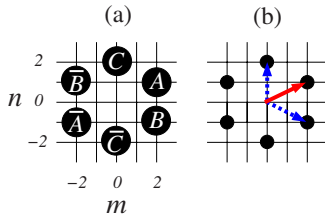
*kontakt@alexander-pinter.de

FIG. 1. (Color online) (a) Dominant modes and their complex conjugates in the Fourier space of Eq. (1). (b) Bilinear coupling of modes B and C (blue dashed arrows) that drive oscillations of mode A (red solid arrow).

A and B are the amplitudes of the marginal L- and R-SPI modes. When both are finite as, e.g., in the SW of the RIB state their nonlinear coupling generates the $m=0$ C mode below its threshold for linear growth: Pure $m=0$ stationary Taylor vortices bifurcate out of the CCF only later on. Although $|C|$ itself remains small compared to $|A|$, $|B|$ in the RIB state its feedback on A, B triggers the Hopf bifurcation of the O-CR-SPI: The oscillations of, say, $|A|$ are driven by bilinear mode couplings of BC as indicated in Fig. 1.

We also use the combined order parameters

$$S = \frac{|A|^2 + |B|^2}{2}, \quad D = \frac{|A|^2 - |B|^2}{2}, \quad \Phi = \theta_C + \theta_B - \theta_A - \pi$$

(2)

that are better suited to describe the bifurcation of the O-CR-SPI with oscillating $D(t)$ and $\Phi(t)$ out of the RIB state, $D=0=\Phi$.

Bifurcation sequence. The pure TW shown by circles in Fig. 2 and the SW solution ($A=B$, $C \neq 0$) marked by diamonds bifurcate at $\mu=0$ out of the unstructured CCF. Initially, the SPI is stable and the RIB is unstable. But then there appears a stable cross-spiral (CR-SPI) solution [triangles in Fig. 2(b)] which transfers stability from the SPI to the RIB. The moduli and phase velocities of these three structures are time independent. At μ_H in Fig. 2 the RIB lose stability in a supercritical Hopf bifurcation to the modulated state of O-CR-SPI. Increasing μ further beyond the range shown in Fig. 2 the O-CR-SPI loses stability at $R_2 \approx -543$ to oscillating structures with azimuthal wave number $M=1$ that are not discussed here.

Dynamics of the modulated SW. Figure 3 shows the temporal variation of characteristic quantities of the O-CR-SPI over one modulation period τ. Thick lines refer to μ immediately above onset μ_H. Thin lines show behavior at a larger value $\mu_>$ (arrow in Fig. 2) that is close to the end of the existence interval of O-CR-SPI. The moduli $|A|$, $|B|$ in Fig. 3(a) and the phase velocities $\dot{\theta}_A$, $\dot{\theta}_B$ in Fig. 3(c) oscillate each in counterphase around a respective common mean. Also $\dot{\theta}_C$ oscillates. Furthermore, $|C|$ and the combined order parameter S show small amplitude oscillations with 2 times the frequency of the other quantities. Close to onset all oscillations are harmonic with $|C|$ and S being practically constant. But at $\mu_>$ the oscillations of $|A|$, $|B|$ and $\dot{\theta}_A$, $\dot{\theta}_B$, Φ have become quite anharmonic, whereas those of S, D, $|C|$, and $\dot{\theta}_C$ are still harmonic. The Fourier spectra in Figs. 4(a)–4(g) of
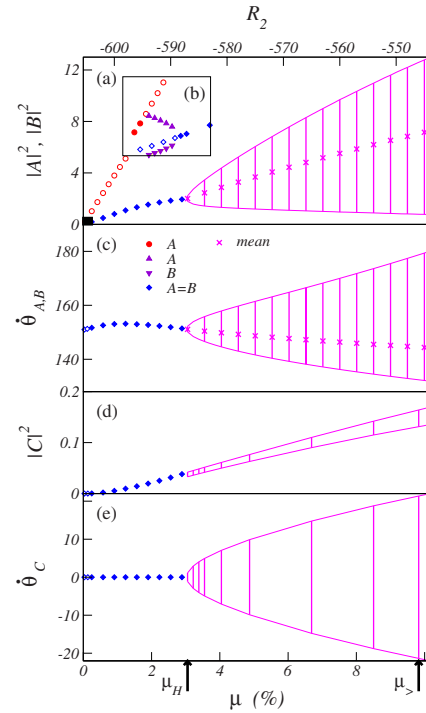

FIG. 2. (Color online) Bifurcation diagrams of SPI (red circles), RIB (blue diamonds), CR-SPI (purple triangles), and O-CR-SPI (mangenta lines and crosses) obtained from numerical simulations of the NSE versus μ and R_2. SPI and CR-SPI are displayed only in (a) and (b); the latter shows the blow-up of the rectangle near the origin of (a). Shown are the squared mode amplitudes $|A|^2$, $|B|^2$ (a), (b) and phase velocities $\dot{\theta}_A$, $\dot{\theta}_B$ (c) of the marginal modes and the same for the nonlinear excited mode C in (d) and (e). Filled (open) symbols denote stable (unstable) solutions with time-independent amplitudes. Crosses refer to temporal averages of the O-CR-SPI. Upper (lower) line shows the maximum (minimum) of the oscillation range indicated by vertical lines. The arrow at μ_H ($R_2=-587$) marks the Hopf bifurcation of the modulated SWs. The second arrow at $\mu=\mu_>$ ($R_2=-546$) is inserted for later reference.

the temporal profiles shown by thin lines in Figs. 3(a)–3(g) reflect this behavior at $\mu_>$.

In the RIB state the phases are such that $\theta_C(t) + \theta_B(t) - \theta_A(t) = \pi$. But as a consequence of the Hopf bifurcation D as well as Φ oscillate in the O-CR-SPI. The squares of their oscillation amplitudes, $\widetilde{D}^2$ and $\widetilde{\Phi}^2$, increase at onset linearly with μ with a subsequent quadratic correction, cf. Figs. 5(c) and 5(d). The monotonous decrease of the modulation period τ is shown in Fig. 5(a). Note that the modulation amplitudes of S in Fig. 5(b) and also of $|C|$ remain very small compared to those of D and Φ.

Amplitude equations. The Hopf bifurcation behavior and the dynamics close to the transition from RIB to O-CR-SPI can be explained and described within a three-mode amplitude-equation approach. It reveals (i) how the rotationally symmetric C mode is generated nonlinearly via the interaction of A and B, i.e., of the $M=2$ SPI constituents in the RIB and (ii) how then C—after it has reached a critical size beyond μ_H—induces amplitude oscillations in A and B.

Invariance under axial translation and reflection of the Taylor-Couette system [5] restricts the form of the three coupled amplitude equations to
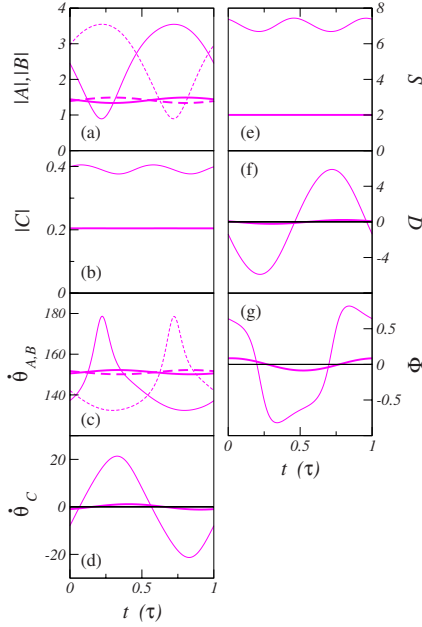
FIG. 3. (Color online) Time variation of O-CR-SPI over one modulation period τ. The left-hand column shows moduli and phase velocities of A, B, and C. In (a) and (c) solid lines refer to A and dashed ones to B. The right-hand column contains the order parameters S, D, and Φ (2). Thick lines are modulation profiles close to the Hopf threshold μ_H and thin lines are those at the larger $\mu_>$ identified by the second arrow in Fig. 2.

$$\dot{A} = AG(|A|^2, |B|^2, |C|^2) + i\kappa BC, \tag{3a}$$

$$\dot{B} = B\hat{G}(|A|^2, |B|^2, |C|^2) + i\kappa A\bar{C}, \tag{3b}$$

$$\dot{C} = CH(|A|^2, |B|^2, |C|^2) + \kappa_0 A\bar{B}. \tag{3c}$$

With $\hat{G}(|A|^2, |B|^2, |C|^2) = G(|B|^2, |A|^2, |C|^2)$ and $H(|A|^2, |B|^2, |C|^2) = \bar{H}(|B|^2, |A|^2, |C|^2)$ the equations are invariant under the operation $(A, B, C) \leftrightarrow (B, A, \bar{C})$, which reflects the axial inversion symmetry $z \leftrightarrow -z$. The functions $G = G' + iG''$ and $H = H' + iH''$ are complex. The superscripts prime and double prime identify the real and imaginary parts, respectively. The coupling constants κ and κ_0 are real.

Since only invariance under translation and reflection along one spatial direction has been used in deriving Eqs. (3) our description of the phenomenon of a SW with oscillating TW components in terms of Eqs. (3) potentially applies to all bifurcating systems with $O(2)$ symmetry in the center manifold, which is quite common.

In the following we discard the coupling term $\kappa_0 A\bar{B}$. It is small in our case and, more importantly, we checked that it is not relevant for driving the Hopf oscillations. They are generated by the coupling terms in (3a) and (3b) as we shall show in the next section.

The mechanism causing the Hopf bifurcation into the modulated SW can be better isolated by rewriting the amplitude equations (3) in terms of the combined order parameters (2),
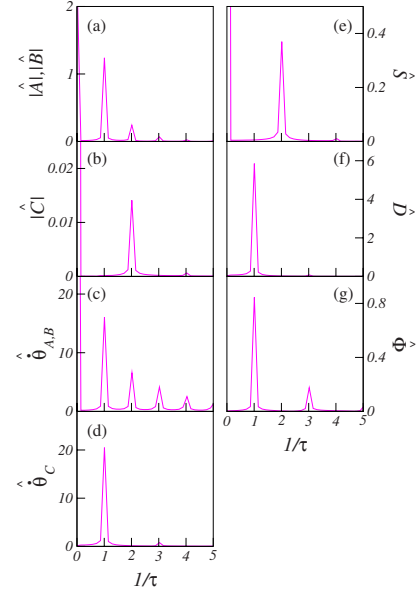

FIG. 4. (Color online) Fourier spectra of the modulation profiles shown by thin lines in Fig. 3 for $\mu = \mu_>$ (cf. arrow in Fig. 2). Note that $|C|$ and S oscillates with 2 times the frequency of the other quantities and that the spectra of $|C|$, S, and D practically do not contain higher harmonics. The spectra of Φ, D, and $\dot{\theta}_C$ ($|C|$ and S) contain only peaks at $(2l+1)/\tau$ $(2l/\tau)$ with $l = 0, 1, 2 \ldots$.

$$\dot{S} = 2(DG'_- + SG'_+), \quad |\dot{C}| = |C|H', \tag{4a}$$

$$\dot{D} = 2(SG'_- + DG'_+) - 2\kappa|C|S^* \sin\Phi, \tag{4b}$$

$$\dot{\Phi} = 2G''_- + 2\kappa\frac{|C|}{S^*}D\cos\Phi - H'', \tag{4c}$$

where $S^* = S\sqrt{1-(D/S)^2} \simeq S$. Here we defined $G_\pm = (G \pm \hat{G})/2$. Note that G_+ and H' (G_- and H'') are even
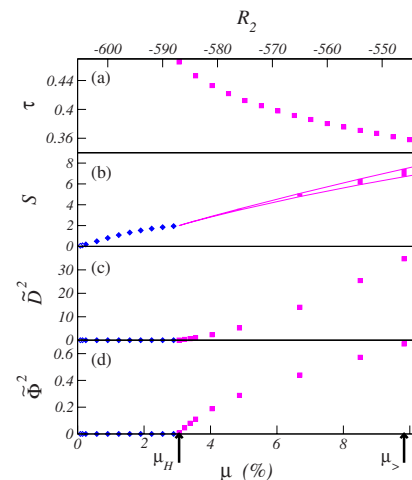

FIG. 5. (Color online) Bifurcation properties of RIB (blue diamonds) and O-CR-SPI (magenta lines and squares) obtained from numerical solutions of the NSE as functions of μ and R_2: (a) Oscillation period τ of the modulation, say, of the moduli $|A|$ and $|B|$ of the O-CR-SPI, (b) S (thin lines delimit the oscillation range indicated by vertical bars), (c) and (d) squared oscillation amplitudes $\tilde{D}$ of D and $\tilde{\Phi}$ of Φ, respectively.

(odd) in D [14] as a result of the inversion symmetry. Hence, Eqs. (4a) are even in D. This in turn explains that S and $|C|$ oscillate with 2 times the frequency of the other quantities in Fig. 3. On the other hand, Eq. (4c) is odd in D and causes the absence of a peak at $2/\tau$ in Fig. 4(g).

We have determined the specific functions G and H for our specific system via fits to the numerically obtained bifurcation branches of SPI, RIB, and CR-SPI in Fig. 2 and to the pure Taylor vortex solution (not shown here) with $A=0=B$, $C\neq 0$, and one-half the spiral wavelength. This produces the bifurcation behavior close to the Hopf threshold well. Note, however, that the Hopf bifurcation is a universal phenomenon of systems like (3) and (4) that is not specific to the Taylor-Couette system. This is most easily understood with the help of the universal small-D expansion of (4) that results from the symmetry properties.

Hopf bifurcation. For small D, i.e., close to the Hopf bifurcation threshold we can use the expansions

$$G_+ = G_+^{(0)} + O(D^2), \quad G_- = G_-^{(1)}D + O(D^3), \tag{5a}$$

$$H' = H'^{(0)} + O(D^2), \quad H'' = H''^{(1)}D + O(D^3). \tag{5b}$$

Here the leading order terms $G_+^{(0)}$, $G_-^{(1)}$, $H'^{(0)}$, $H''^{(1)}$ still depend on S and $|C|^2$. Inserting (5) into (4) and using the smallness of Φ yields a simplified model that is linear in D,

$$\dot{S} = 2SG_+'^{(0)}, \quad |\dot{C}| = |C|H'^{(0)}, \tag{6a}$$

$$\dot{D} = 2(SG_-'^{(1)} + G_+'^{(0)})D - 2\kappa|C|S\Phi, \tag{6b}$$

$$\dot{\Phi} = \left(2G_-''^{(1)} + 2\kappa\frac{|C|}{S} - H''^{(1)}\right)D. \tag{6c}$$

It explains the Hopf bifurcation out of the RIB state and the O-CR-SPI properties close to onset. For example, S and $|C|$ are virtually constant because they are decoupled from D and Φ in the model equations (6). Furthermore, Eq. (6c) shows that Φ is enslaved by D and that the phase shift between them is $\tau/4$ as to be seen in Fig. 3 close to μ_H. This justifies the solution ansatz

$$D(t) = \tilde{D}\cos(\omega_H t), \quad \Phi(t) = \tilde{\Phi}\sin(\omega_H t), \tag{7}$$

where ω_H is the Hopf frequency.

The latter is identified together with the bifurcation threshold μ_H by a linear stability analysis of the RIB fixed point $D=0=\Phi$, $S=S_{\mathrm{RIB}}(\mu)$, $C=C_{\mathrm{RIB}}(\mu)$ for which $G_+'^{(0)}=0$ according to Eq. (6a). Thus, the linearized equations for the stability-relevant deviations from this fixed point read $\dot{D}=aD+b\Phi$, $\dot{\Phi}=cD$, with coefficients $a=2SG_-'^{(1)}$, $b=-2\kappa|C|S$, $c=2G_-''^{(1)}+2\kappa\frac{|C|}{S}-H''^{(1)}$ to be taken at the RIB fixed point. Consequently, the location of the zero in $a(\mu)$ determines μ_H and the imaginary part of the eigenvalue at μ_H, i.e., the Hopf frequency is then given by $\omega_H^2=-bc\propto\kappa+$h.o.t. (where h.o.t. stands for higher order terms), revealing that the coupling terms in (3a) and (3b) cause the Hopf bifurcation. Furthermore, $a(\mu)=\alpha(\mu-\mu_H)$ with positive α to ensure decay of oscillations below μ_H and growth above it.

Conclusion. The bifurcation of a spiral vortex structure with oscillating TW amplitudes out of an SW is shown to be triggered by the coupling to a nonlinearly excited mode when the latter exceeds a critical strength. Since this state, in which the TW amplitudes oscillate in counterphase around a common mean occurs quite robustly in a relatively wide parameter range, it should be easily accessible to experiments.

Our results have been obtained by full numerical simulations and explained and confirmed by a coupled amplitude equation model that captures the mode coupling between two symmetry degenerate critical modes and a nonlinearly excited one. Our bifurcation scenario can occur in all systems with an $O(2)$ symmetric center manifold, arising, for example, in systems with translation and inversion symmetry, which is a quite general one. It has therefore the potential to occur also in other structure-forming systems, say, in hydrodynamics, chemical reactions, or biological systems, etc., where any two symmetry degenerate basic modes A and B couple similarly to a third one, C, that is nonlinearly excited by them and that destroys the $A=B$ state once C has reached a critical size.

[1] M. C. Cross and P. C. Hohenberg, Rev. Mod. Phys. **65**, 851 (1993).

[2] M. Golubitsky and I. Stewart, Arch. Ration. Mech. Anal. **87**, 107 (1985).

[3] Y. Demay and G. Iooss, J. Mec. Theor. Appl. 193 (1984), special supplement.

[4] A. Pinter, M. Lücke, and Ch. Hoffmann, Phys. Rev. Lett. **96**, 044506 (2006).

[5] P. Chossat and G. Iooss, *The Couette-Taylor Problem* (Springer, Berlin, 1994).

[6] R. Tagg, Nonlinear Sci. Today **4**, 1 (1994).

[7] Ch. Hoffmann, M. Lücke, and A. Pinter, Phys. Rev. E **69**, 056309 (2004).

[8] Stable RIBs were found [9] in a long system of aspect ratio $\Gamma=36$ with radius ratio $\eta=0.727$ where theory [3,5] and numerical simulations [9] predicted a subcritical transition.

RIBs in end-plate-dominated short systems ($\Gamma<10$, $\eta=1/2$) were recently reported [10] to come with two different symmetries [11].

[9] R. Tagg, W. S. Edwards, H. L. Swinney, and P. S. Marcus, Phys. Rev. A **39**, 3734 (1989).

[10] J. Langenberg, G. Pfister, and J. Abshagen, Phys. Rev. E **68**, 056308 (2003); Phys. Fluids **16**, 2757 (2004).

[11] E. Knobloch and R. Pierce, in *Ordered and Turbulent Patterns in Taylor-Couette Flow*, edited by C. D. Andereck and F. Hayot (Plenum, New York, 1992), p. 83.

[12] A phase diagram of SPI, RIB, CR-SPI, and O-CR-SPI for $\lambda=1.3$ and an investigation of the wave-number dependence of the bifurcation porperties is provided in [13].

[13] A. Pinter, M. Lücke, and Ch. Hoffmann, Phys. Rev. E **78**, 017303 (2008).

[14] To see that, write $f(|A|^2,|B|^2)=f(S+D,S-D)$.